

Engineering the Pupil Phase to Improve Image Quality

S. Prasad^a, T. C. Torgersen^b, V. P. Pauca^b, R. J. Plemmons^c, and J. van der Gracht^d

^aCenter for Advanced Studies, University of New Mexico, Albuquerque, NM, 87131

^bDepartment of Computer Science, Wake Forest University, Winston-Salem, NC 27109

^cDepartments of Computer Science and Mathematics, Wake Forest University, Winston-Salem, NC 27109

^dHolospex, Inc., 6470 Freetown Rd., Suite 200-104, Columbia, MD 21044

ABSTRACT

By suitably phase-encoding optical images in the pupil plane and then digitally restoring them, one can greatly improve their quality. The use of a cubic phase mask originated by Dowski and Cathey to enhance the depth of focus in the images of 3-d scenes is a classic example of this powerful approach. By using the Strehl ratio as a measure of image quality, we propose tailoring the pupil phase profile by minimizing the sensitivity of the quality of the phase-encoded image of a point source to both its lateral and longitudinal coordinates. Our approach ensures that the encoded image will be formed under a nearly shift-invariant imaging condition, which can then be digitally restored to a high overall quality nearly free from the aberrations and limited depth of focus of a traditional imaging system. We also introduce an alternative measure of sensitivity that is based on the concept of Fisher information. In order to demonstrate the validity of our general approach, we present results of computer simulations that include the limitations imposed by detector noise.

Keywords: Pupil-phase mask, wavefront coding, integrated imaging, Strehl ratio, Fisher information, focus extension, image quality, nonlinear optimization.

1. INTRODUCTION

In a seminal paper,¹ Dowski and Cathey proposed the use of a cubic phase mask in the pupil of a standard, limited-focus imaging system to encode a 3-dimensional object which can then be digitally restored. Under suitable conditions, such restored images exhibit excellent depth-dependent detail, although without any phase encoding, such detail would be washed out because of the normal focus-dependent blur. Furthermore, the restoration comes with no penalty to the total light flux or the spatial bandwidth of the imaging system.

Previously,² we introduced the concept of pupil phase engineering (PPE), which is a procedure to optimize the design of a more general pupil-phase mask that can lead to even better performance than the cubic mask in extending the depth of focus. The approach we specifically discussed uses the Strehl ratio (SR) as a metric of performance of such integrated optical-digital imaging systems. By forcing the first few derivatives of the SR with respect to the defocus parameter to be small without degrading its actual value greatly, we argued for a better optimized phase mask. Preliminary numerical simulations we presented in Ref² demonstrated the generally superior performance of such engineered masks when compared to the cubic.

In the present paper, we elaborate further on the SR based optimization and compare it with a new PPE approach that uses the full point spread function (PSF), not just its on-axis value that defines the SR. From the many possible metrics involving the full PSF, we choose one that is based formally on the concept of Fisher information (FI) used in statistical estimation theory.⁴ The FI furnishes, as we shall see, a particularly simple measure of focus independence. It also has the merit of having been studied extensively over the past several decades, and its rich theoretical framework may enable a deeper understanding of the general subject of pupil-phase encoding. The use of FI in the context of imaging is not new. It has been previously discussed in the context of estimation of a variety of object parameters from noisy image data, including the estimation of the object when its range is unknown.⁵ Also, Dowski and Cathey¹ used FI to evaluate the cubic phase mask in

Send correspondence to S. Prasad: E-mail: sprasad@unm.edu, Telephone: 1 505 277 5876

the spatial-frequency domain. Here, we use FI in the physical domain to furnish an optimization criterion for deducing the best phase mask under a range of imaging conditions.

The present work is limited to the use of PPE to treat the problem of focus extension. The PPE concept is more general, however, and can be employed for a number of other useful applications that range from static aberration control to a reduction of focal depth.⁶

The rest of the paper is organized as follows. We consider in Sec. 2 a number of classes of pupil phase masks that can be employed to remove the defocus blur in a well corrected imaging system. In Sec. 3, we introduce our two main PPE approaches, based on the SR and FI metrics, and discuss their implementation. The results of numerical optimization within each of the various classes of phase masks are presented in Sec. 4. Section 5 is devoted to a comparison of the various phase masks based on the independence of the SR from defocus, as a measure of focus insensitivity of the imaging system, and on the variation of the in-focus MTF with spatial frequency, as a measure of restorability of encoded images. We describe in Sec. 6 a model three-dimensional cone shaped object for which we have performed computer simulations of its phase encoded and restored images for the various pupil masks of interest here. The results of these computer simulations are discussed in Sec. 7 where we demonstrate the effectiveness of our PPE approach in removing the defocus blur by considering the mean square error as a metric for the quality of restored images. Some concluding remarks appear in Sec. 8.

2. PUPIL PHASE MASKS

A number of phase profiles can be employed in the pupil to encode images of objects possessing a finite depth coordinate. The original proposal¹ argued for a cubic phase mask based on the requirement that the phase $\phi(x, y)$ be monomial in the pupil coordinates (x, y) , be separable in those coordinates, and lead to an MTF that is asymptotically focus-independent. By contrast, our PPE approach calls for a more general pupil function based on requirements we place in the physical domain, namely those based on the PSF. In view of the greater generality of our approach, we discuss a number of classes of phase functions within which we can optimize the encoding pupil phase.

The most general polynomial form of the phase $\phi(x, y)$ is the following:

$$\phi(x, y) = \sum_{m=0}^{\infty} \sum_{n=0}^{\infty} a_{mn} x^m y^n. \quad (1)$$

We henceforth exclude the constant (a_{00}) and linear (a_{10}, a_{01}) terms, which represent piston and tip-tilt phases that are of no consequence here. A useful regrouping of terms in Eq. (1) that is suggestive of various optical aberrations is furnished by the Zernike polynomials. The different low-order Zernikes which we have investigated,² along with their names, are listed below.

$Z_4(\rho, \theta)$	$= \sqrt{3}(2\rho^2 - 1)$	defocus
$Z_5(\rho, \theta)$	$= \sqrt{6}\rho^2 \sin 2\theta$	astigmatism, 45°
$Z_6(\rho, \theta)$	$= \sqrt{6}\rho^2 \cos 2\theta$	astigmatism, 0°
$Z_7(\rho, \theta)$	$= \sqrt{8}(3\rho^3 - 2\rho) \sin \theta$	coma, x-direction
$Z_8(\rho, \theta)$	$= \sqrt{8}(3\rho^3 - 2\rho) \cos \theta$	coma, y-direction
$Z_9(\rho, \theta)$	$= \sqrt{8}\rho^3 \sin 3\theta$	field curvature, 30°
$Z_{10}(\rho, \theta)$	$= \sqrt{8}\rho^3 \cos 3\theta$	field curvature, 0° ,

where the polar coordinates (ρ, θ) are simply related to the Cartesian coordinates, $x = \rho \cos \theta$, $y = \rho \sin \theta$. We employ a truncated version of expansion (1) that uses only low order Zernike polynomials. Since terms linear in x, y occur in a number of these polynomials, we normally subtract out such terms from our expansion before optimizing it.

Symmetry arguments can help constrain the form of the phase function further. If we require that the phase function be optimized equally relative to the x and y coordinate axes, then it must be invariant under an $x \leftrightarrow y$ exchange operation. Excluding the constant and linear terms, we then have the following form for ϕ :

$$\phi(x, y) = axy + b(x^2 + y^2) + c(x^3 + y^3) + d(x^2y + xy^2) + \dots \quad (2)$$

where the ellipses represent fourth and higher-order terms. It is easy to see that there are at most $(\lfloor n/2 \rfloor + 1)$ terms in the n th order, where $\lfloor x \rfloor$ is the largest integer less than or equal to x . The number of terms with $x \leftrightarrow y$ symmetry at a given order thus grows only linearly with the order, while the total number of terms at a given order without such symmetry would do so quadratically.

Further constraints on the phase can be placed by requiring that it be odd under coordinate inversion, $\phi(-x, -y) = -\phi(x, y)$. Such phase forms, as we show in Ref.³ lead to Strehl ratios and PSF's that are both even in the defocus parameter. This evenness implies that the Taylor expansions of these quantities only contain even powers of defocus. This is desirable since all odd powers are automatically absent and do not require any optimization considerations.

3. OPTIMIZING THE PUPIL PHASE: THEORY

We adopt two different strategies to determine the actual coefficients in the various forms of the pupil phase we have just discussed. They are both based on considerations of the PSF $h(\mathbf{r}; \tau)$ in the image plane (coordinate vector: $\mathbf{r} = (x_i, y_i)$),

$$h(\mathbf{r}; \tau) = |K(\mathbf{r}; \tau)|^2, \quad (3)$$

where K is the following pupil integral:

$$K(\mathbf{r}; \tau) = \frac{1}{\lambda f \sqrt{A}} \int d^2 \rho P(\rho) e^{i[\frac{2\pi}{\lambda f} \mathbf{r} \cdot \rho + \phi(\rho) + \tau \rho^2]}. \quad (4)$$

In this expression, $P(\rho)$ is the pupil function, equal to 1 inside the pupil and 0 outside for a clear pupil, $\phi(\rho)$ is the pupil phase above and beyond the defocus phase $\tau \rho^2$, $\mathbf{r} \cdot \rho$ denotes the dot product of vectors \mathbf{r} and ρ , λ is the wavelength of illuminating light, f is the focal length, and A is the area of the pupil. The pupil vector ρ has the coordinates x, y . The use of vector notation lends brevity to the formulas.

3.1. Strehl-Ratio Based Optimization

The Strehl ratio (SR) is the ratio of the on-axis values of the PSF with and without the pupil phase. For phase masks that are odd under parity (or coordinate inversion, $x \rightarrow -x$, $y \rightarrow -y$, *i.e.*, $\rho \rightarrow -\rho$),

$$\phi(-\rho) = -\phi(\rho), \quad (5)$$

the following expression for the SR may be derived:

$$\chi(\tau) = \frac{1}{A^2} \int \int d^2 \rho d^2 \sigma P(\rho) P(\sigma) \cos \phi(\rho) \cos \phi(\sigma) \cos[\tau(\rho^2 - \sigma^2)]. \quad (6)$$

The τ -dependent cosine term may now be expanded in its Taylor series to yield the following even-power series for the SR:

$$\chi(\tau) = \sum_{n=0}^{\infty} \chi_{2n} \tau^{2n}, \quad (7)$$

where the coefficients χ_{2n} have the value

$$\chi_{2n} = \frac{(-1)^n}{n!} \frac{1}{A^2} \int \int d^2 \rho d^2 \sigma P(\rho) P(\sigma) \cos \phi(\rho) \cos \phi(\sigma) (\rho^2 - \sigma^2)^{2n}. \quad (8)$$

A use of the binomial expansion

$$(\rho^2 - \sigma^2)^{2n} = \sum_{m=0}^{2n} (-1)^m \binom{2n}{m} \rho^{2m} \sigma^{4n-2m} \quad (9)$$

then reduces the double-pupil-integral form (8) to one involving only *single* pupil integrals,

$$\chi_{2n} = \frac{(-1)^n}{n!} \sum_{m=0}^{2n} (-1)^m \binom{2n}{m} C_{2m} C_{4n-2m}, \quad (10)$$

where

$$C_\ell = \frac{1}{A} \int d^2\rho P(\boldsymbol{\rho}) \rho^\ell \cos[\phi(\boldsymbol{\rho})] \equiv \langle \rho^\ell \cos[\phi(\boldsymbol{\rho})] \rangle, \quad (11)$$

the triangular brackets indicating an average of the quantity they enclose over the pupil function.

Our optimization procedure is based on making the terms labeled by $n = 1, \dots, (N - 1)$ in expansion (7) small, for some chosen N , so that the first significant τ -dependent term of that expansion is $O(\tau^{2N})$, subject to “regularization” constraints on the magnitude of the SR at $\tau = 0$, namely on χ_0 , and the parameters of the pupil phase $\phi(\boldsymbol{\rho})$. We implement this procedure by seeking to minimize the squared norm of the vector $(\chi_2, \dots, \chi_{2N-2})$ to which are added appropriate regularization terms.

For pupil phases that are not odd under any of the symmetries (coordinate inversion being one such) of the pupil function $P(\boldsymbol{\rho})$, odd powers in τ also occur in the expansion (7) (see Ref³ for a detailed discussion of the symmetries of the PSF), and the expression for the coefficients χ_n is also more involved² than Eq. (10). The preceding optimization procedure must be accordingly modified.

3.2. Fisher-Information Based Optimization

The Fisher-information (FI) metric we propose uses the full PSF, rather than just its on-axis value that defines the SR. Any odd-parity phase mask gives rise to a PSF that, like the SR, has the desirable property of containing no odd powers of the defocus parameter τ . The following expression for the PSF explicitly demonstrates this fact:

$$h(\mathbf{r}; \tau) = \frac{1}{A^2} \int \int d^2\rho d^2\sigma P(\boldsymbol{\rho}) P(\boldsymbol{\sigma}) \cos\left[\frac{2\pi}{\lambda f} \mathbf{r} \cdot (\boldsymbol{\rho} - \boldsymbol{\sigma}) + \phi(\boldsymbol{\rho}) - \phi(\boldsymbol{\sigma})\right] \times \cos[\tau(\rho^2 - \sigma^2)]. \quad (12)$$

The Fisher information that measures the sensitivity of the PSF to defocus may be defined as⁴

$$\begin{aligned} J_I(\tau) &= \int h(\mathbf{r}; \tau) \left[\frac{\partial \ln h(\mathbf{r}; \tau)}{\partial \tau} \right]^2 d^2r \\ &= \int \frac{1}{h(\mathbf{r}; \tau)} \left[\frac{\partial h(\mathbf{r}; \tau)}{\partial \tau} \right]^2 d^2r. \end{aligned} \quad (13)$$

Instead of the squared norm of the vector of coefficients of the SR, we can seek to minimize the sum of $J_I(\tau = 0)$ and the usual regularizing terms. The problem with such a simple approach is that $J_I(\tau)$ vanishes identically for zero defocus, $\tau = 0$, for any odd-parity phase mask, since the PSF has no $O(\tau)$ terms in its Taylor expansion. We could define J_I in such situations to be relative to the squared-defocus parameter, $\tau_2 \equiv \tau^2$, not τ , noting that $J_I(\tau_2)$ does not vanish at $\tau = 0$, in general, for *any* phase mask. Alternatively, we could use, instead of $J_I(0)$, the following integral of $[J_I(\tau)]^2$:

$$I(\tau_0) = \int_{-\tau_0}^{\tau_0} [J_I(\tau)]^2 d\tau, \quad (14)$$

where $(-\tau_0, \tau_0)$ denotes the (symmetric) range of defocus parameters of interest for the physical problem at hand. In this paper, we use only the metric (14) for all FI-based optimizations of the pupil phase mask.

In both SR and FI based approaches, additive regularization terms are essential to constrain the choice of the optimal phase mask from reaching the trivial, physically uninteresting solution of an infinitely large phase and an identically vanishing PSF. We therefore constrain our optimization procedure by requiring that the resulting SR not fall below a minimum threshold value, determined essentially by how robust the restoration algorithm is against falling SR values in the presence of noise. The following Fermi-Dirac regularization term implements this requirement:

$$J_\chi(\mathbf{u}) = M(1 - \chi(0, \mathbf{u})) \frac{1}{e^{k[\chi(0, \mathbf{u}) - \bar{\chi}]} + 1}, \quad (15)$$

where $\chi(0, \mathbf{u})$ is the Strehl ratio at zero defocus, \mathbf{u} is the vector of phase-mask coefficients being sought, M is a positive constant representing the maximum penalty, k is a large positive constant that determines the steepness of the “cutoff edge,” and $\hat{\chi}$ represents the minimum acceptable SR. For small SNR, both k and $\hat{\chi}$ are expected to scale inversely with SNR.

A numerically improved form of FI (13) is possible in which the divergence of the integrand at positions \mathbf{r} where the PSF vanishes is explicitly removed. This form for J involves the complex amplitude $K(\mathbf{r}; \tau)$ whose squared modulus is the PSF. In terms of K and K^* , given by Eq. (4) and its complex conjugate, expression (13) for $J_I(\tau)$ may be cast in the form

$$\begin{aligned} J_I(\tau) &= \int \frac{1}{KK^*} \left(K \frac{\partial K^*}{\partial \tau} + K^* \frac{\partial K}{\partial \tau} \right)^2 dx dy \\ &= \int \left[\frac{K}{K^*} \left(\frac{\partial K^*}{\partial \tau} \right)^2 + \frac{K^*}{K} \left(\frac{\partial K}{\partial \tau} \right)^2 + 2 \frac{\partial K}{\partial \tau} \frac{\partial K^*}{\partial \tau} \right] dx dy. \end{aligned} \quad (16)$$

Note that the ratio K/K^* is unimodular and finite, being equal to $\exp[2i \arg(K)]$.

4. OPTIMIZING THE PUPIL PHASE: NUMERICAL RESULTS

A number of classes of masks have been considered in our work. We present details of optimization for symmetric mixed cubic masks of form (2) with $a = b = 0$, although results corresponding to optimized Zernike masks discussed earlier² will also be used for comparison.

4.1. Strehl-Ratio Based Optimization Results

Since the symmetric mixed mask of degree 3 has two independent coefficients c and d , one can in general hope for at most two of the SR derivatives, χ_{2n} , to be made as small as we please. Since in general there are a whole infinite set of solution pairs (c, d) possible and both the sensitivity of the SR to defocus and the SR decrease with increasing $|c|, |d|$, only one or at most a few of these solutions pairs will be optimal in the sense of meeting the requirement of maximum possible insensitivity to defocus consistent with the constraint of a minimum SR threshold. The purpose of the nonlinear optimizer is to find these optimal solutions approximately by minimizing the objective function

$$J_{SR}(c, d) = [\chi_2(c, d)]^2 + [\chi_4(c, d)]^2 + M[1 - \chi_0(c, d)] \frac{1}{e^{k[\chi_0(c, d) - \hat{\chi}]} + 1}. \quad (17)$$

An additional penalty term of form $\gamma[c^2 + d^2]$ can be added to prevent the coefficients from becoming too large. However, we usually ignore such a term in our calculations.

The objective function is highly oscillatory with numerous local minima in the (c, d) plane. A Monte-Carlo type technique is therefore used for the global optimization. Uniformly random starting points were chosen in a closed region $\mathcal{R} = [-50, 50] \times [-50, 50]$, and the Levenberg-Marquardt method was applied to find a corresponding local minimum of the objective function (17) for each starting point. A total of 500 starting points were chosen. The set of solutions were sorted according to the Strehl-based metric, excluding the penalty term. The solution with the lowest value for the Strehl metric (most insensitivity to defocus) that lies on or near the boundary implied by the penalty term (greatest strength possible satisfying the Strehl constraint) was selected.

The optimal solution found for the symmetric basis of total degree three is given by:

$$(c, d) = (36.5961, -50.3604),$$

i.e., the pupil phase mask is given by the function:

$$\phi(x, y) = 36.5961 (x^3 + y^3) - 50.3604 (x^2 y + x y^2). \quad (18)$$

The minimum value of the objective function corresponding to the coefficients in equation (18) is the squared Euclidean norm of the following vector:

$$\mathbf{fvec} = [1.04659e - 08, 5.82893e - 08, 2.33977e - 06]$$

The components of the vector \mathbf{fvec} are χ_2 , χ_4 , and $J_\chi(c, d)$, respectively.

The values of χ_2 and χ_4 , proportional to the second and fourth derivatives of SR with respect to defocus, are *very* small. Thus, we should expect very good insensitivity to defocus in this example, and the simulation tests support this, as we shall see later. For this filter, we can also see some geometric distortion. This should come as no surprise and no disappointment, since the Strehl based metric really can not measure distortion with respect to defocus. The full PSF in this example resembles the PSF of filters we have seen in previous work using the Zernike basis as well. However, the expediency of a low-dimensional parameter search characteristic of the symmetric filter as well as its overall simplicity make it a superior choice to the Zernike filter.

4.2. Fisher-Information Based Optimization Results

A similar Monte-Carlo approach of starting the Levenberg-Marquardt method of minimization with uniformly random starting points in the closed region $\mathcal{R} = [-50, 50] \times [-50, 50]$ of the (c, d) plane was applied in this case as well. The objective function $J(c, d)$ is different, however, and given by the expression

$$J(c, d) = \sum_{\tau \in S} [J_I(\tau)]^2 + J_\chi(c, d) \quad (19)$$

where $J_I(\tau)$ is the Fisher information discussed earlier, S is a set of defocus (τ) values of interest, and $J_\chi(c, d)$ is the penalty function used previously to enforce a minimum Strehl ratio. The set S of values of τ is chosen to be

$$S = \{1, 3, 5, 7, 9, 11, 13, 15, 17, 19\}. \quad (20)$$

The sum in Eq. (19) approximates the integral of $[J_I(\tau)]^2$ over the range (0,19) in τ , or equivalently half of that integral over the range (-19, 19) since $J_I(\tau)$ is even in τ for the symmetric filter.

A total of 40 uniform random starting points were chosen, and the solutions were sorted according to the Fisher Information based metric in equation (19), excluding the penalty term. The solution with the lowest value for the Fisher Information metric (most insensitivity to defocus) that lies on or near the boundary implied by the penalty term (greatest strength possible satisfying the Strehl constraint) was selected. The optimal solution found for the symmetric basis of total degree three is given by:

$$a = [32.6809, -102.027],$$

i.e., the pupil phase mask is given by the function:

$$\phi(x, y) = 32.6809 (x^3 + y^3) - 102.027 (x^2y + xy^2) \quad . \quad (21)$$

The minimum value of the objective function corresponding to the coefficients in equation (21) is the squared Euclidean norm of the following vector:

$$\mathbf{fvec} = [\quad 0.00105885, 0.00363798, 0.00569221, 0.00899365, 0.0127826, \\ \quad 0.0166305, 0.02045, 0.0241882, 0.0275795, 0.0307985, 0.00837011]$$

The first 10 components of \mathbf{fvec} correspond to the Fisher information metric function $J_I(\tau)$ for the values of $\tau \in S$ defined in (20). The last component of \mathbf{fvec} corresponds to the $J_\chi(c, d)$ penalty term in Eq. (19) The values of $J_I(\tau)$ are small, so we can hope for good insensitivity to defocus.

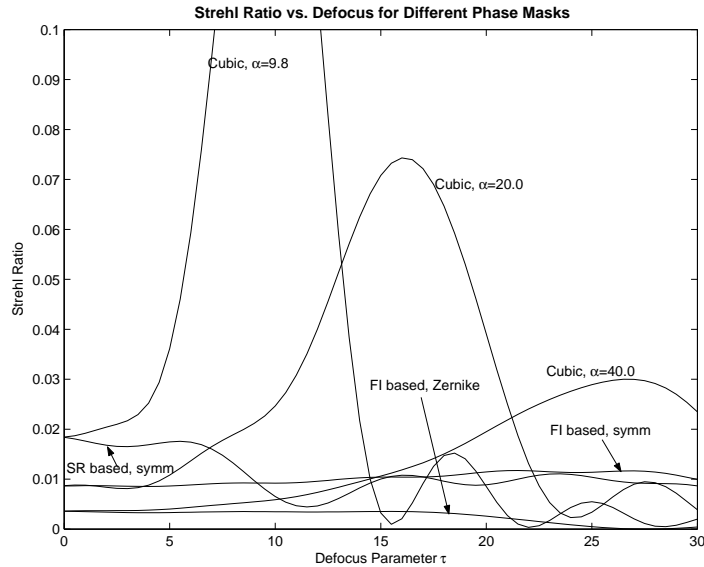


Figure 1. Strehl Ratio versus defocus for a number of phase masks. The masks and the values of their coefficient parameters are specified in the text.

5. SR AND MTF BASED COMPARISONS OF VARIOUS OPTIMIZED PHASE MASKS

Before addressing the relative performance of the various phase masks in the imaging of a simulated three-dimensional object, we evaluate them in terms of two elementary metrics of image quality, namely their Strehl ratio and MTF values. For this comparison, we choose the two symmetric mixed cubic phase masks optimized according to our SR and FI based metrics of the previous section as well as the SR-optimized Zernike phase mask of Ref² and the pure cubic mask of Ref.¹ The two symmetric mixed cubic masks refer to the mask given by Eq. (2) with $a = b = 0$. The values of c and d are 32.6809 and -102.027 for the FI optimized mask and 36.5961 and -50.3604 for the SR-optimized mask. For the chosen Zernike mask, the only non-vanishing coefficients of the Zernike polynomials in the phase mask are those for Z_5, \dots, Z_{10} ; they are determined in Ref² to be $-0.007581, 0.1349, -3.707, 3.512, 0.5899, 0.7914$, respectively. For the pure cubic mask, three different strengths were chosen for which the same in-focus SR values as for the optimized symmetric mixed cubic and Zernike masks are obtained. These cubic mask strengths were found to be close to 9.8, 20, and 40.

In Fig. 1, we plot the Strehl ratio as a function of the defocus parameter τ for the various masks described above. Note the essentially flat SR vs. defocus curves for both the FI optimized and Zernike cases, reflecting excellent optimization. The pure cubic mask does not exhibit good focus independence for small to moderate defocus values, except for the highest-strength case.

A somewhat different comparison uses the MTF as a metric of both focus invariance and of image restorability. We concentrate here on the image restorability alone, by plotting the discretized form of the angularly averaged in-focus MTF, namely

$$M(\nu) = \frac{1}{2\pi} \int_0^{2\pi} |H(\nu, \theta)| d\theta, \quad (22)$$

where $H(\nu, \theta)$ is the in-focus OTF expressed in polar coordinates in which ν is the magnitude of the spatial frequency and θ is the azimuthal angle of the spatial-frequency vector. In Fig. 2, we display this average as a function of ν for the same six masks that were used in the previous figure. In all cases, this mean MTF seems to be well off the zero floor at nearly all frequencies that are not too close to the cut-off, but the pure cubic filters have generally the highest MTF in the mid frequency range in all cases. Notwithstanding this observation, we may not use it to make any robust judgements about which filter will lead to better restorability of three-dimensional objects. That is so for two reasons. First, what is needed for good restoration is that the MTF values simply be

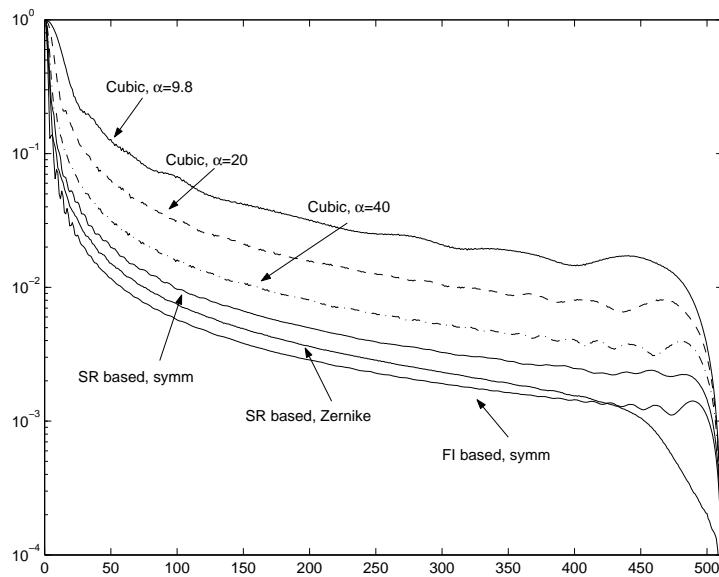


Figure 2. Angularly averaged in-focus MTF as a function of spatial frequency (in pixel units), for the six masks of the previous figure.

well above the noise floor over the frequencies of interest. A study of the noise floor which separates a certain signal space of larger MTF values from a certain noise space of smaller MTF values is currently under way. Second, the MTF is only half the story. What is of importance is also the phase of the OTF, which together with MTF determines the full PSF, and it is the focus invariance of the full PSF, or equivalently of the full OTF, that is of greater relevance to the focus extension problem. Pure cubics, while ensuring good focus invariance of the MTF, do suffer from the problem of having a highly depth-dependent phase for their OTF.

Our FI optimized filters work with the full PSF, and furthermore take both the defocus range and overall SNR value into consideration. They are thus likely to provide the highest depth of focus in the phase-encoded image. The correspondingly excellent focus invariance of the PSF should then lead to restorations that should resolve the depth detail well. This expectation is verified in Sec. 7 where we simulate a three-dimensional object, image it with different optical systems containing the different pupil phase masks we have discussed here, and then restore the optical images.

6. COMPUTER MODELING AND OPTICAL SYSTEM SIMULATION

Numerically computed filter designs are tested using a computer simulation software system developed by the authors. The simulator models a parabolic cone-shaped object surrounded by a set of wings arranged in a spiral at equal angles and linearly progressive distances away from a reference plane coincident with the center point. The central point is thus visually nearest the observer, while the wings spiral away in the counter-clockwise direction. Each point in the object is blurred by a spatially-varying PSF which models the appropriate defocus according to the distance from that point to the reference plane. For improved performance, the modeled object is decomposed into point sets which are equidistant from the reference plane (and thus equally blurred). The usual Fourier transform based convolution methods are applied to each point set. The simulated scattered light energy from each point set is then summed together to produce the final simulated image.

Figure 3 illustrates the effect of noise-free spatially varying defocus. For comparison, a theoretical blur-free perspective projection of the object is also shown on the left. The authors' software simulates the effect of a pupil-phase encoding filter by adding a chosen fixed pupil-phase function to the defocus (quadratic) phase as each point set is processed.

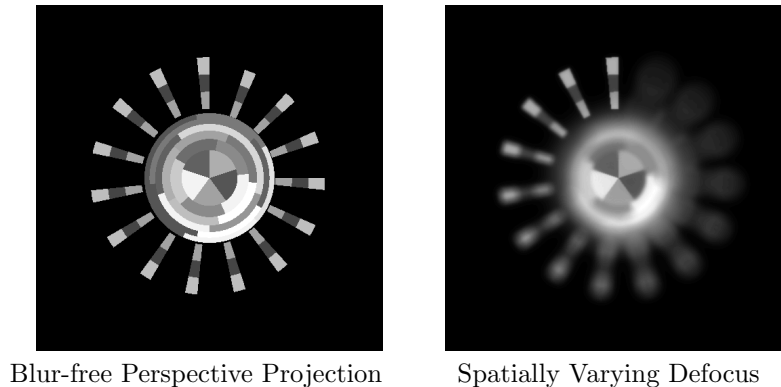


Figure 3. Simulated Parabolic Cone Shaped Object.

7. PUPIL PHASE ENCODING AND IMAGE RESTORATION

The PPE optimization we have described in Secs. 3 and 4 makes no reference to the object being imaged. Rather it is based on a balancing of the focus insensitivity of the PSF with a minimum SR by nonlinear optimization techniques. We now describe how faithfully images of the simulated cone object encoded by these optimized phase masks can be restored by a simple Wiener filter under a given SNR estimate.

In Figs. 4 and 5, we display the phase encoded image, the PSF of the encoding pupil phase mask of form (2), and the restored image. Additive Gaussian noise with an overall SNR of 100 was assumed in our simulations. The restoration uses a regularized Wiener filter with regularization parameter $4e - 06$. Figure 4 employs the SR optimized symmetric mixed cubic mask with coefficients $a = b = 0, c = 36.5961, d = -50.3604$, while Figure 5 employs the corresponding FI optimized mask with coefficients $a = b = 0, c = 32.6809, d = -102.027$. For comparison, we exhibit in Figure 6 the restorations with a pure cubic filter of strength 20 and 40, respectively. The pure cubic of strength 20 has the same in-focus SR as the FI optimized mask, while the cubic of strength 40 was used here to see if and how much the performance improves by raising the cubic-mask strength. Note the visually superior restoration with the FI optimized mask, for which not only is the SR most independent of defocus (see Fig. 1), but the PSF has a rather compact form with approximate triangular symmetry.

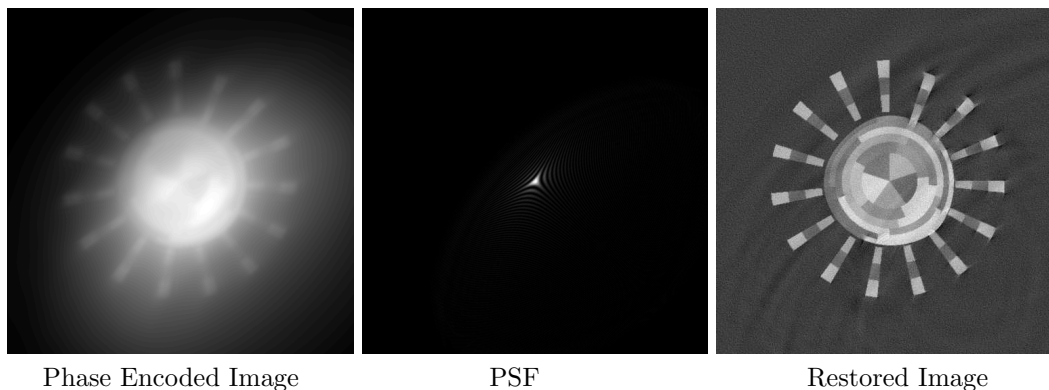


Figure 4. The phase-encoded blurred image, the PSF, and the restored image for the SR-optimized filter described in the text.

Visual impressions can often be deceptive, however. We therefore use a more objective criterion for ranking the restored images, that of taking the root mean squared error (RMSE) over the entire image. The RMSE per pixel, Δ , is defined as follows:

$$\Delta^2 = \frac{1}{N^2} \sum_{m=1}^N \sum_{n=1}^N [\hat{f}(m, n) - f(m, n)]^2, \quad (23)$$

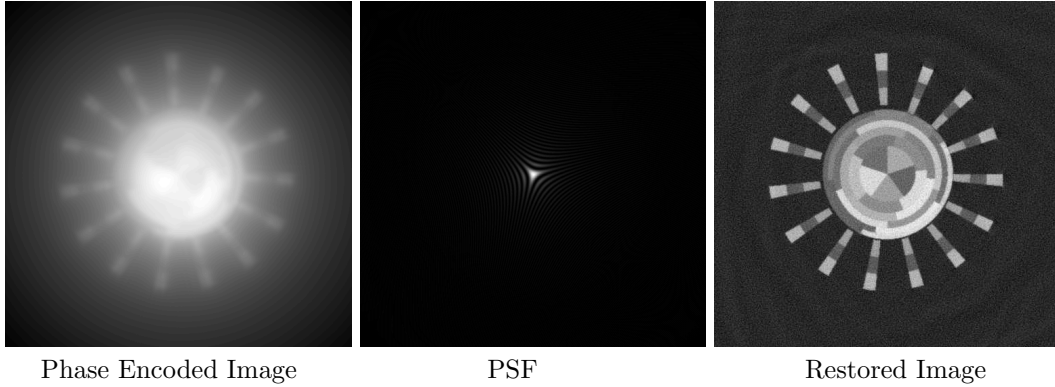


Figure 5. The phase-encoded blurred image, the PSF, and the restored image for the FI-optimized filter described in the text.

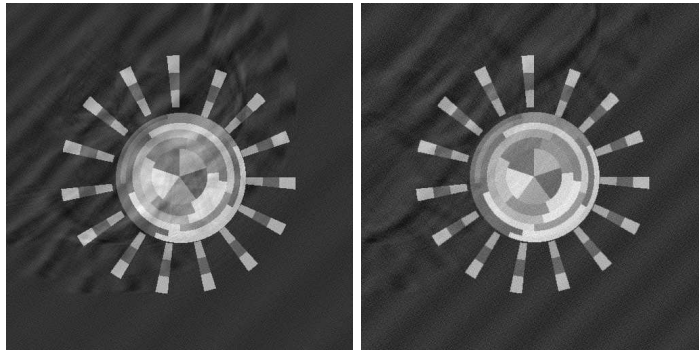


Figure 6. The restored images for a pure cubic filter, with cubic strength 20 (left) and 40 (right)

where the images are on an $N \times N$ square pixel array, and $\hat{f}(m, n)$ and $f(m, n)$ are, respectively, the restored image and model object intensities at the pixel (m, n) .

We use the RMSE as a metric to compare the restorations of images encoded by our two optimized filters and by suitably chosen pure cubic filters. A preliminary choice of the strengths of the pure cubic mask is based on the simple requirement laid out in Sec. 5, namely that the in-focus SR for the pure cubic be the same as the in-focus SR for the two PPE optimized symmetric mixed cubic masks we have computed here. This single-parameter search was performed by computing the in-focus SR for a range of cubic strength values and inferring, by simple bisection interpolation, that strength value that has the correct SR.

In Figs. 7 and 8, we display the difference images, each formed by subtracting the restored image from the true object, for the SR and FI optimized symmetric mixed cubic masks and two pure cubics of strength 20 and 40. The RMSE-per-pixel values in the Wiener restored images for the four masks in the order listed above are 0.0690, 0.0570, 0.0785, and 0.0658, respectively. Since the peak intensity value at a pixel in the model object was 0.906, these mean errors amount to 7.6%, 6.2%, 8.7%, and 7.3%, respectively, of that peak value. The FI based symmetric mixed cubic mask thus outperforms the other three masks in this preliminary test, a fact that is also confirmed by the visual appearance of the various difference images. Raising the cubic strength does improve the restorations, but a fairer comparison of the performances of the symmetric mixed cubic and pure cubic filters requires applying the same exact optimization with which we compute the former to the latter filters. This work is in progress at present.

To date, researchers have emphasized direct linear methods such as the Wiener filter, to restore wavefront coded images^{1,7} because of good computational efficiency that allows for real-time restoration. This has been the approach adopted in the present paper too. In many applications, real-time results are essential and direct methods are used. In some applications, however, direct linear methods should be used only to identify regions

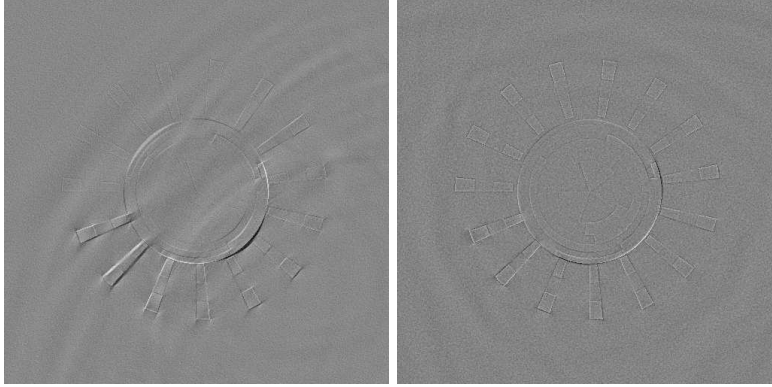


Figure 7. Simulated Difference Image (True Object Minus Restored Image) for the SR optimized (left) and FI optimized symmetric mixed cubic masks (right)

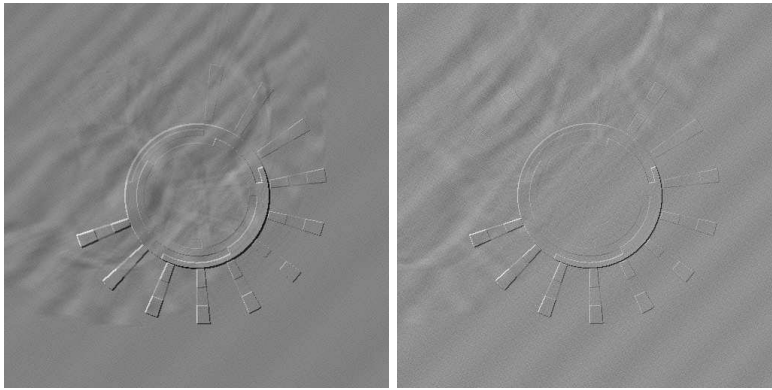


Figure 8. Simulated Difference Image (True Object Minus Restored Image) for a pure cubic mask of strength 20 (left) and of strength 40 (right)

of interest in real-time and more computationally intensive iterative algorithms could be subsequently applied in an attempt to improve restoration fidelity.⁸ A preliminary study of iterative restoration of wavefront coded imagery for focus invariance has recently been given in Ref.⁹ A more exhaustive study of this problem will appear in a future paper.

8. CONCLUSIONS AND FUTURE WORK

The present work generalizes our earlier investigations² where we introduced the concept of pupil phase engineering, which is a new mathematical approach to optimize the choice of pupil phase masks to improve the quality of digitally restored images. Two optimization metrics of particular interest to the problem of extending the depth of focus that we have considered here are the Strehl ratio and the Fisher information. Our basic approach is to seek good focus insensitivity of the PSF, subject to a minimum acceptable Strehl ratio needed for image restoration under given conditions of detection noise and over the range of defocus values of interest. Achieving the right balance between focus insensitivity and acceptable restorability requires solving a nonlinear optimization problem in this approach.

Although the originally proposed cubic phase mask performs well under a wide range of conditions and has the advantage of simplicity, a more general polynomial mask can be better optimized to meet a more specific set of performance demands. The proposed PPE approach can, in fact, be regarded as providing a general framework in which to address a broad range of image improvement objectives, ranging from extension and reduction of the depth of focus to ameliorating any image degradations that arise from optical aberrations.

Assessing the relative effectiveness of the various phase masks in improving the quality of restored images under a variety of operating conditions and for different classes of objects will be a major focus of future work. We have also begun investigating several iterative restoration methods to deblur pupil-phase encoded imagery in order to explore more fully both the trade-off space of speed, accuracy, and robustness and the parameter space of SNR, defocus range, noise statistics, and mask parameters.

ACKNOWLEDGMENTS

We gratefully acknowledge funding support from the Army Research Office under grant DAAD19-00-1-0540 and from the Air Force Office of Scientific Research under grants F49620-01-1-0321 and F49620-02-1-0107. We have also benefited from discussions with Harsha Setty.

REFERENCES

1. E.R. Dowski and W.T. Cathey, "Extended depth of field through wavefront coding," *Applied Optics*, Vol. 34, pp. 1859-1866, 1995.
2. S. Prasad, T. Torgersen, V.P. Pauca, and R. Plemmons, "Integrated Optics Systems for Image Quality Control," *Proc. 2002 AMOS Technical Conference, Maui, HI, Sep 2002*.
3. S. Prasad, T. Torgersen, V.P. Pauca, R. Plemmons, and J. van der Gracht, "Optimizing the Pupil Phase for Image Quality Control," in preparation.
4. H. Van Trees, *Detection, Estimation, and Modulation Theory*, Wiley, 1968.
5. E. R. Dowski, "An info theoretic approach to incoherent information processing systems," published on-line at www.cdm-optics.com/wave/pubs/papers/info/paper.html.
6. S. Sherif and T. Cathey, "A phase grating to reduce the depth of field of incoherent hybrid imaging systems," in *OSA Trends in Optics and Photonics (TOPS), Integrated Computational Imaging Systems*, OSA Technical Digest, Washington, D.C., 2001.
7. S. Bradburn, E.R. Dowski and W.T. Cathey, "Realizations of focus invariance in optical-digital systems with wavefront coding," *Applied Optics*, Vol. 26, pp. 9157-9166, 1997.
8. J. Nagy, P. Pauca R. Plemmons, and T. Torgersen, "Space-varying restoration of optical images," *J. Optical Soc. Amer. A.*, Vol. 14, pp. 3162-3174, 1997.
9. J. van der Gracht, J. Nagy, P. Pauca, and R. Plemmons, "Iterative restoration of wavefront coded imagery for focus invariance," in *OSA Trends in Optics and Photonics (TOPS), Integrated Computational Imaging Systems*, OSA Technical Digest, Washington, D.C., 2001.